Supplementary Information (SI) for ChemComm.
This journal is © The Royal Society of Chemistry 2025

Supporting Information for

Biligand synergistic MOFs with dual enhancements in stability and charge transfer for efficient CO_2 photoreduction

Jiayin Tao,[a] Yujun Ouyang,[a] Kai Zhang,[a] Keke Wang,*[a] Bolin Zhou,[a] Xiahe Chen,[a] Yi Zhang,[b] Junze Zhao,[a] Qin Wang,[a] Yun-Fang Yang,[a] Jiexiang Xia,*[c] Huaming Li [c] and Yuanbin She *[a]

[a] State Key Laboratory of Green Chemical Synthesis and Conversion, College of Chemical Engineering, Zhejiang University of Technology, Hangzhou 310014, China. E-mail: wangkk@zjut.edu.cn; sheyb@zjut.edu.cn

[b] Department of Applied Physics, The Hong Kong Polytechnic University, Kowloon, Hong Kong 999077, P. R. China

[c] School of Chemistry and Chemical Engineering, Institute for Energy Research, School of the Environment and Safety Engineering, Jiangsu University, Zhenjiang 212013, PR China. E-mail: xjx@ujs.edu.cn

Contents

1. Experimental procedures

1.1. Materials

Zirconium chloride ($ZrCl_4$, ≥99.9%), acetic acid (AR), 2,2'-bipyridine-5,5'-dicarboxylic acid (H_2BPYDC, 98%) are purchased from Shanghai Maclean's Biochemical Technology Co. Ltd. N,N-dimethyl formamide (DMF, ≥99.5%), methanol (≥99.7%), dimethyl sulfoxide (DMSO, 99.7%), acetone (≥99.5%), hydrogen fluoride (AR, ≥40.0%) are supplied by Shanghai Sinopharm Chemical Reagent Co., Ltd. All the chemicals were used without any purification.

1.2. Synthesis of 3,3'-bis(trifluoromethyl)-4,4'-biphenyldicarboxylic acid ($H_2BPDC\text{-}2CF_3$)

$H_2BPDC\text{-}2CF_3$ was synthesized as in our previous work.[1]

1.3. Synthesis of UiO-67-CF_3-X

A mixture of $ZrCl_4$ (0.233 g, 1.00 mmol), DMF (40 mL), and acetic acid (3.603 g, 60.00 mmol) was added to a Teflon inner liner and sonicated for 10 min. Subsequently, mixed ligands with varying molar ratios of $H_2BPDC\text{-}2CF_3$ (x mmol, x = 1.00, 0.75, 0.50, 0.25, and 0.00) and H_2BPYDC (1-x mmol) were added to the autoclave, followed by another 10 min sonication. The mixture was then sealed in a stainless steel-autoclave, heated to 120 °C and maintained at this temperature for 72 h. After cooling to room temperature, the resulting MOF solid was collected by centrifugation and sequentially washed with DMF (2 × 200 mL), DMSO (4 × 200 mL), methanol (4 × 200 mL), and acetone (2 × 200 mL). Finally, the MOF solid was dried at 100 °C under vacuum overnight, named as UiO-67-CF_3-X (X = 100, 75, 50, 25, and 0, where X represents the molar percentage of $H_2BPDC\text{-}2CF_3$ in the total ligand content).

2. Characterization and measurement

Fourier transform infrared (FT-IR) spectra were recorded on a Nicolet 6700 spectrometer in the range of 4000–500 cm^{-1} using KBr pellets. Powder X-ray diffraction (XRD) patterns were collected on a PANalytical Empyrean diffractometer equipped with Cu Kα radiation (λ = 1.5406 Å) in reflection mode. Thermogravimetric analysis (TGA) was performed on a NETZSCH TG 209 F1 Libra instrument under an air atmosphere at a heating rate of 10 °C·min^{-1} from 30 to 600 °C. The morphology of the samples was characterized using a GeminiSEM 500 field-emission scanning electron microscope (SEM). X-ray photoelectron spectroscopy (XPS) measurements were carried out on a Thermo Scientific K-Alpha spectrometer with Al Kα excitation, and all binding energies were calibrated using the C 1s peak at 284.8 eV. Nitrogen adsorption–desorption isotherms were measured at 77 K on a Micromeritics ASAP 2460 analyzer to determine the specific surface area and pore structure. Prior to analysis, the samples were degassed under vacuum at 120 °C for 12 h. UV–visible diffuse reflectance spectra (UV–Vis DRS) were obtained on a Shimadzu UV-3600 spectrophotometer using $BaSO_4$ as a reference. Photoluminescence (PL) spectra were recorded on a Hitachi F-7000 fluorescence spectrophotometer; samples were dispersed in deionized water (5 mg in 5 mL) via ultrasonication, and emission spectra were collected under 240 nm excitation. Using the JES-FA200 instrument, the electron paramagnetic resonance (EPR) signal of the sample was obtained. Water surface contact angle measurements were performed with a Dataphysics OCA20.

All electrochemical tests for the UiO-67-CF_3-X samples were conducted on a CHI 660E electrochemical workstation using a standard three-electrode configuration: an Ag/AgCl reference electrode, a platinum counter electrode, and a working electrode prepared as described below. Mott–Schottky (M–S) and electrochemical impedance spectroscopy (EIS) measurements were performed in a 0.1 M KCl aqueous solution containing 5 mM $K_3[Fe(CN)_6]$, while transient photocurrent response (i–t) curves were measured in a 0.5 M Na_2SO_4 aqueous solution. Catalyst ink was prepared by dispersing 4 mg of sample powder in a mixture of 600 μL deionized water, 400 μL anhydrous ethanol, and 80 μL Nafion solution, followed by ultrasonication to achieve a homogeneous dispersion. For i–t measurements, 200 μL of the ink was coated onto FTO glass; for EIS, 10 μL was drop-cast onto carbon cloth; and for M–S tests, 5 μL was loaded onto a carbon rod electrode.

3. Photocatalytic CO_2 reduction measurement

The photocatalytic CO_2 reduction testing was performed in a Labsolar-6A closed gas system. The catalysts (30mg) were dispersed in pure water (50 mL). Prior to Xe lamp irradiation (Microsolar300D, Perfectlight, China), the reaction system underwent multiple CO_2 purging cycles to ensure complete displacement of atmospheric gases. The system was filled with high-purity CO_2 (0.08 MPa) Temperature control at 5 °C was achieved via a recirculating chiller system (equipped with condensate water circulation) throughout the photocatalytic process. A fully automatic online gas chromatograph instrument (Cotrun GC2002) was used to quantify the products.

For the recycling experiments, the photocatalyst was recovered by centrifugation and washed three times with deionized water and acetone after each CO_2 photoreduction reaction. It was then dried in a vacuum oven at 80 °C and subjected to subsequent cyclic CO_2 photoreduction tests under identical conditions.

In the photocatalytic $^{13}CO_2$ reduction test, isotope tracing was performed using a mixed $^{13}CO_2/^{12}CO_2$ feed under identical conditions, and the products were analyzed by gas chromatography-mass spectrometry (Agilent 8890/7000D).

To determine oxidation products, after photocatalytic CO_2 reduction over UiO-67-CF_3-50, the reaction solution was centrifuged to separate the solid photocatalyst. The supernatant (500 μL) was then mixed with 2 mL of 0.1 M KI and 50 μL of 0.01 M $H_{24}Mo_7N_6O_{24}\cdot 4H_2O$. After 10 min, the concentration of hydrazine in the reaction solution was determined using a calibration curve.

4. Density functional theory calculation methods

All calculations were performed using the Gaussian 16 package.[2] Geometry optimizations, as well as calculations of frontier molecular orbitals (FMOs) and their energies, were conducted with the ωB97XD functional,[3] employing the def2-TZVP basis set for all atoms.[4]

5. Characterization results

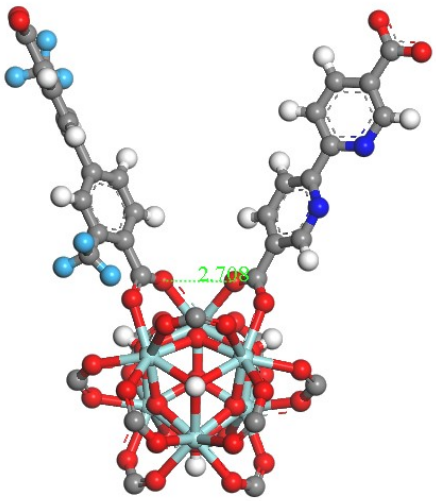

Fig. S1. The O-O distance between the carboxylate groups of BPDC-2CF_3 and BPYDC in UiO-67-CF_3-X.

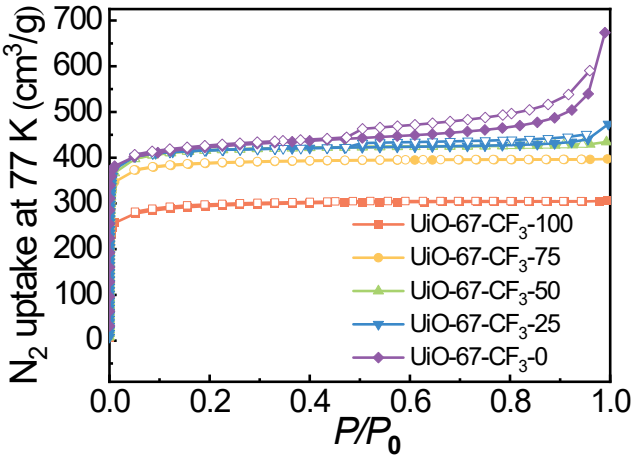

Fig. S2. N_2 adsorption-desorption isotherms of UiO-67-CF_3-X.

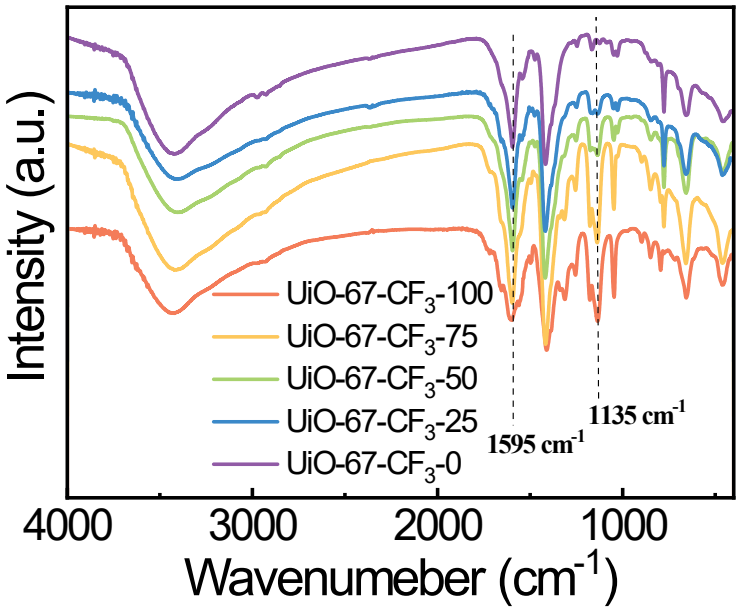

Fig. S3. FT-IR spectra of UiO-67-CF_3-X.

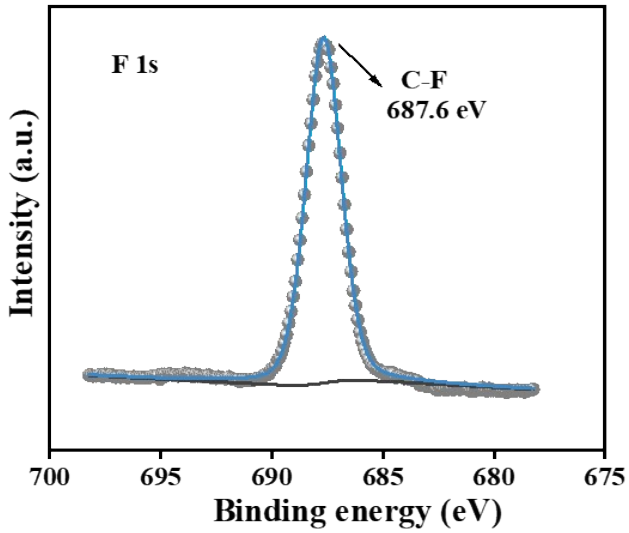

Fig. S4. F 1s XPS spectrum of UiO-67-CF_3-100.

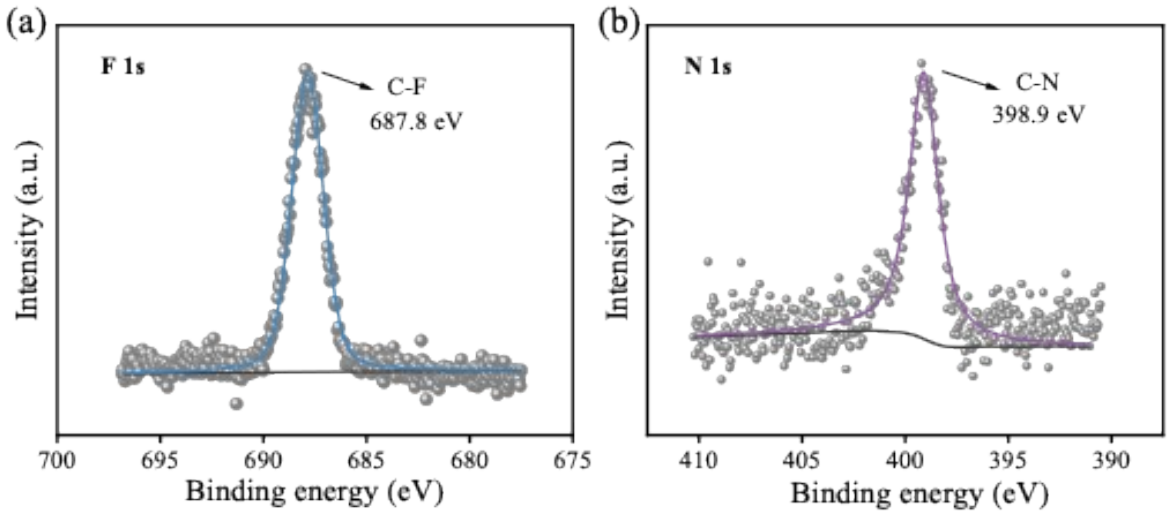

Fig. S5. (a) F 1s and (b) N 1s XPS spectra of UiO-67-CF_3-75.

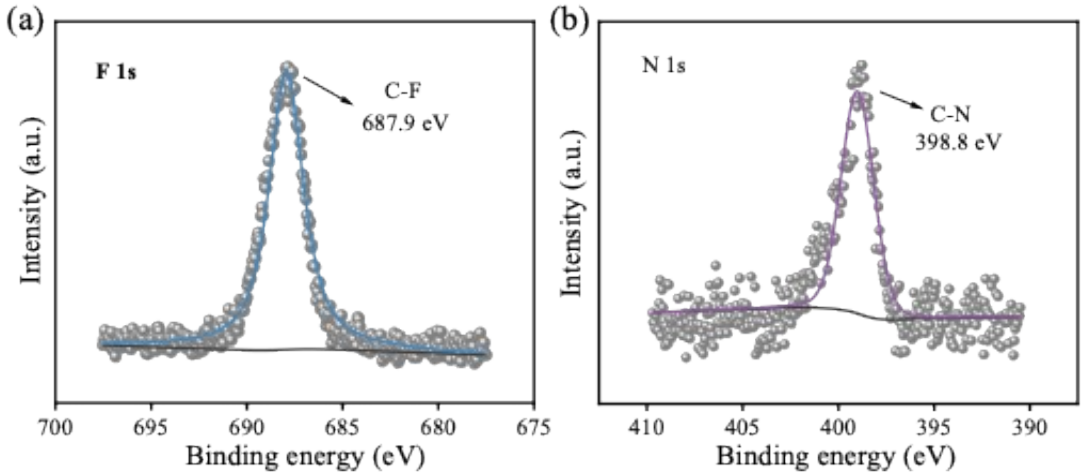

Fig. S6. (a) F 1s and (b) N 1s XPS spectra of UiO-67-CF_3-50.

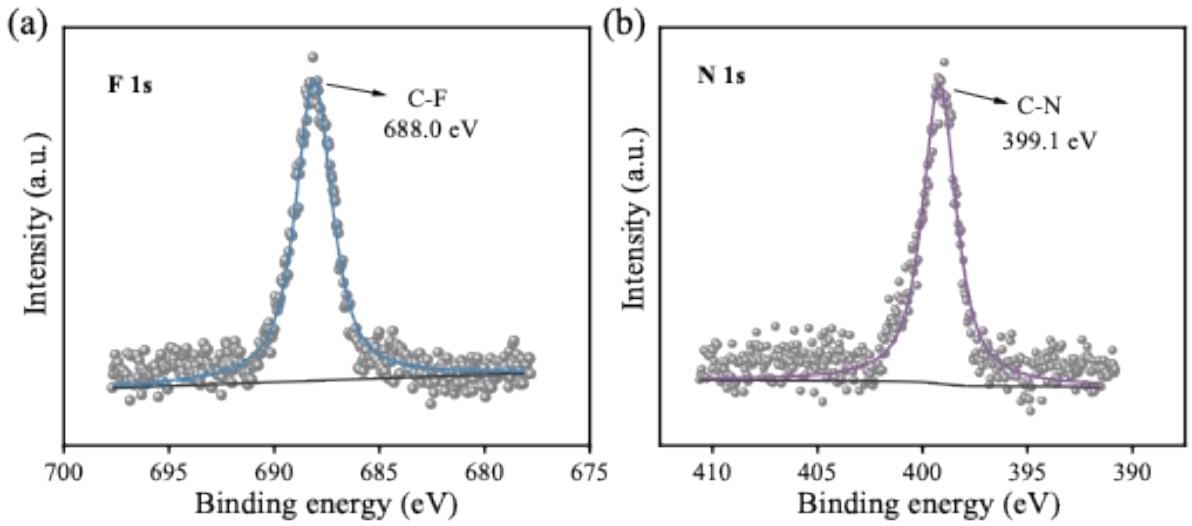

Fig. S7. (a) F 1s and (b) N 1s XPS spectra of UiO-67-CF_3-25.

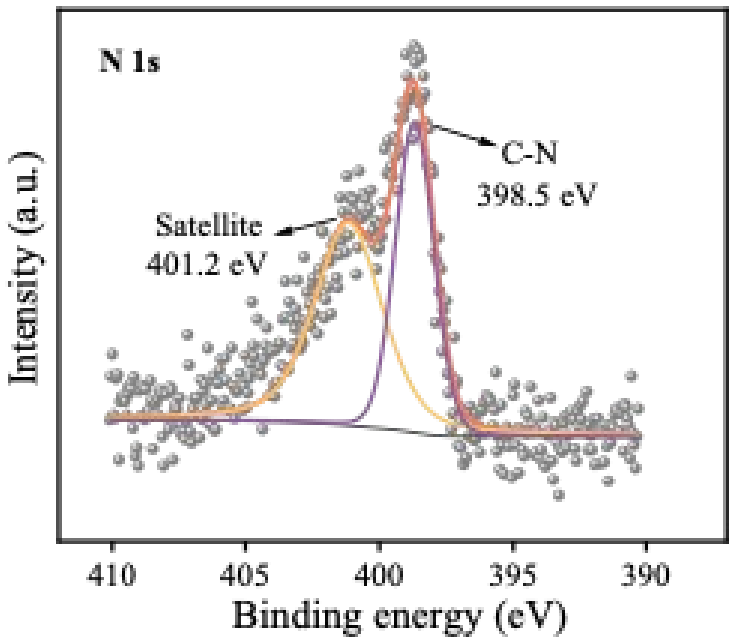

Fig. S8. N 1s XPS spectrum of UiO-67-CF_3-0.

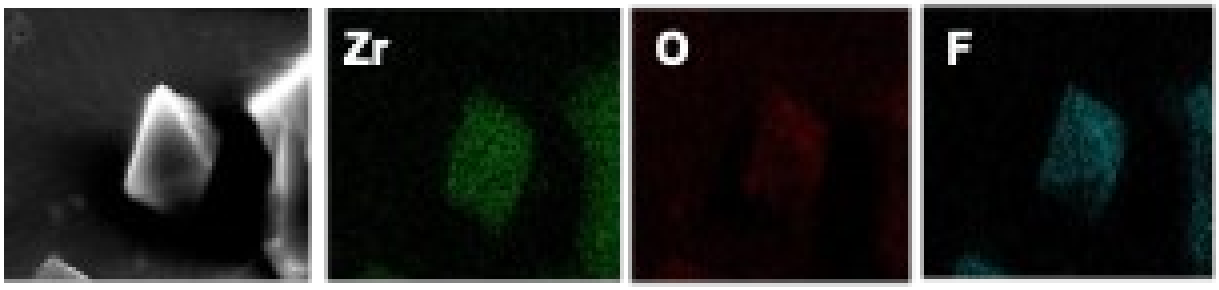

Fig. S9. SEM image and the corresponding energy-dispersive X-ray spectroscopy elemental mapping of UiO-67-CF_3-100.

Fig. S10. SEM image and the corresponding energy-dispersive X-ray spectroscopy elemental mapping of UiO-67-CF_3-75.

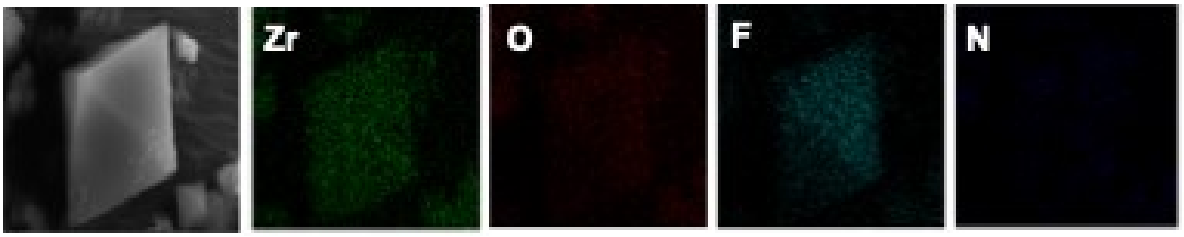

Fig. S11. SEM image and the corresponding energy-dispersive X-ray spectroscopy elemental mapping of UiO-67-CF_3-50.

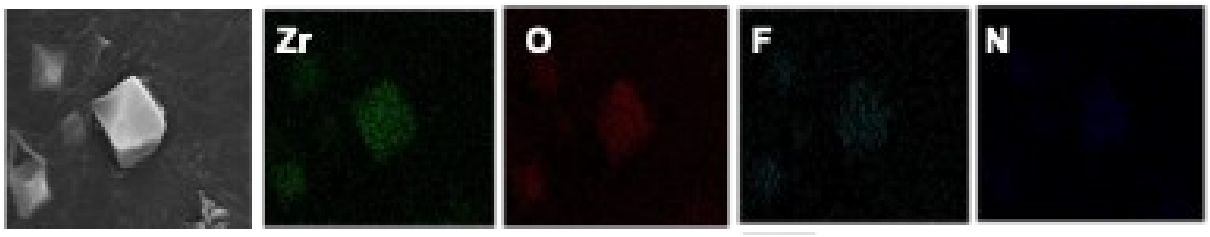

Fig. S12. SEM image and the corresponding energy-dispersive X-ray spectroscopy elemental mapping of UiO-67-CF_3-25.

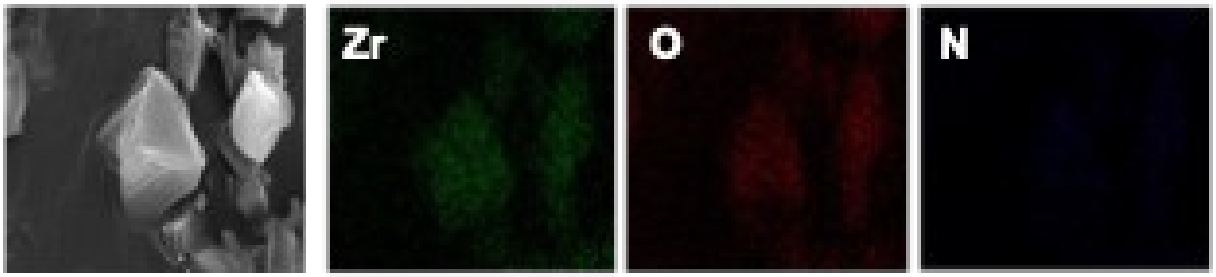

Fig. S13. SEM image and the corresponding energy-dispersive X-ray spectroscopy elemental mapping of UiO-67-CF_3-0.

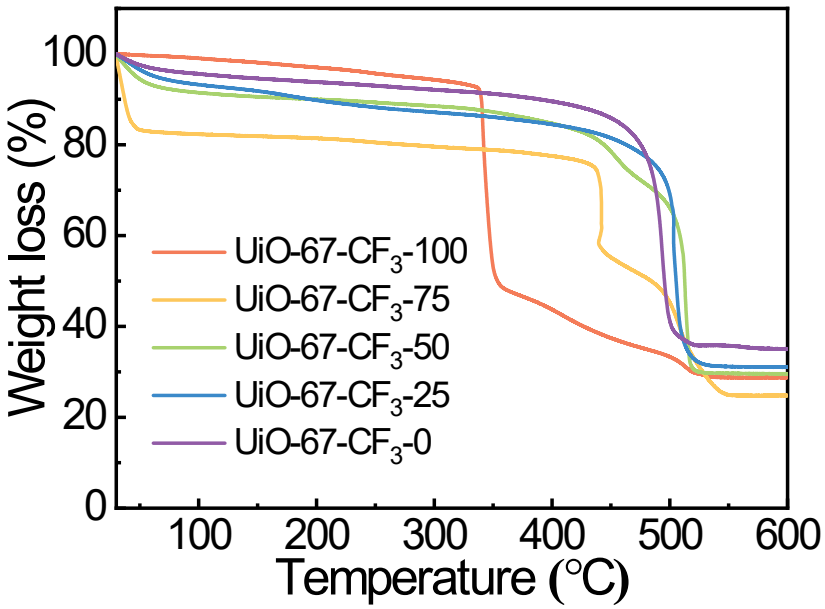

Fig. S14. TGA curves of UiO-67-CF3-X.

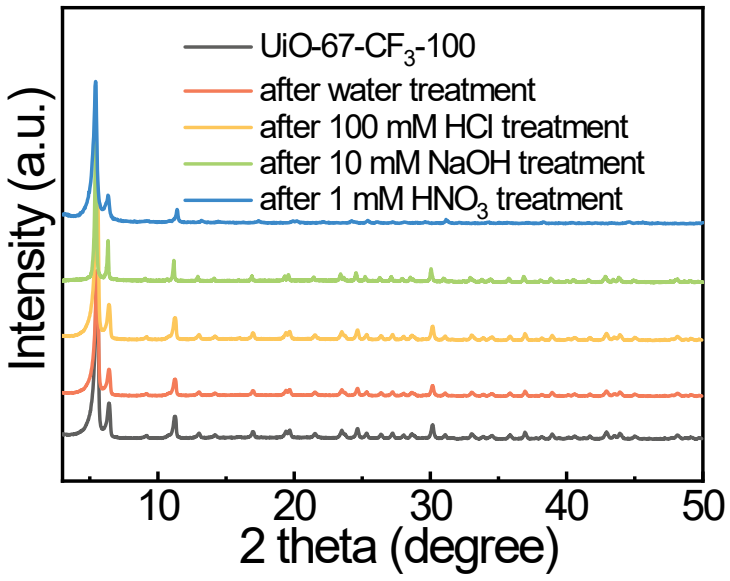

Fig. S15. PXRD patterns of UiO-67-CF_3-100 after treatment.

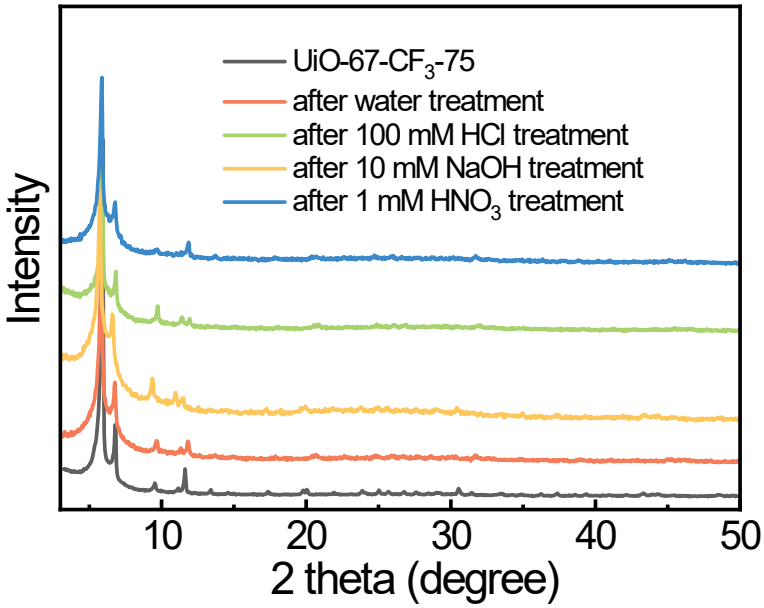

Fig. S16. PXRD patterns of UiO-67-CF_3-75 after treatment.

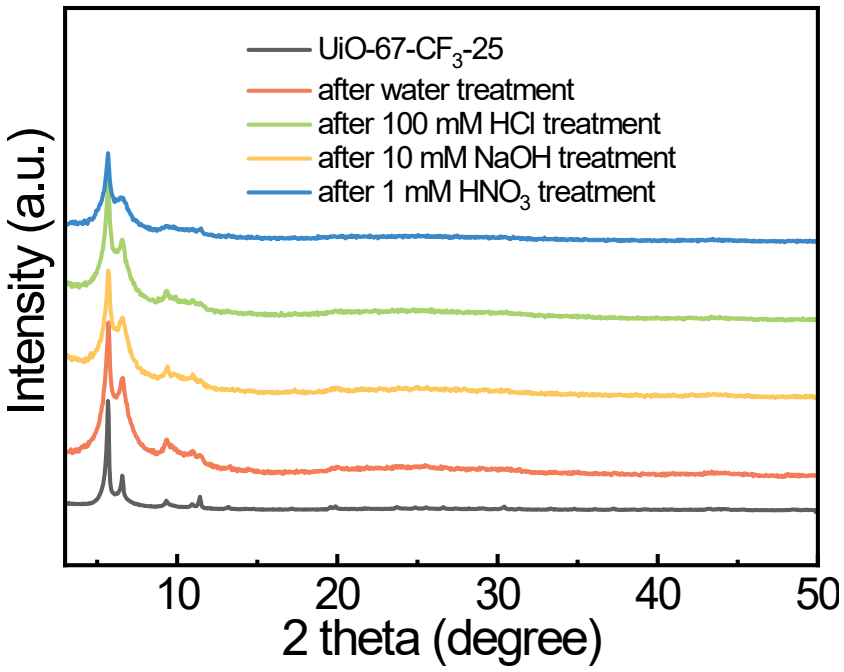

Fig. S17. PXRD patterns of UiO-67-CF_3-25 after treatment.

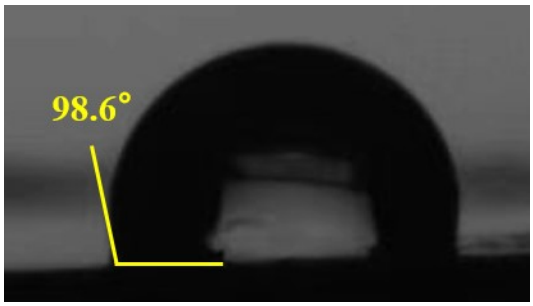

Fig. S18. Water contact angle on UiO-67-CF_3-100.

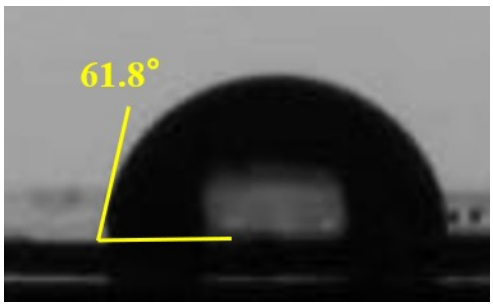

Fig. S19. Water contact angle on UiO-67-CF_3-75.

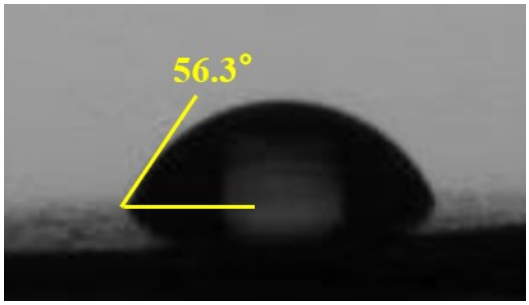

Fig. S20. Water contact angle on UiO-67-CF_3-50.

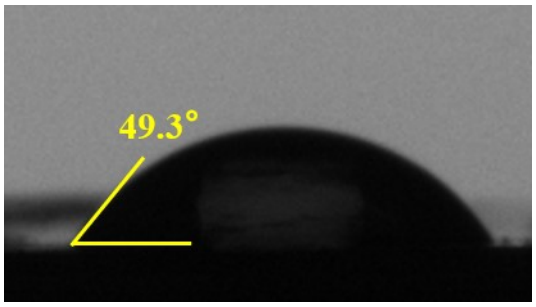

Fig. S21. Water contact angle on UiO-67-CF_3-25.

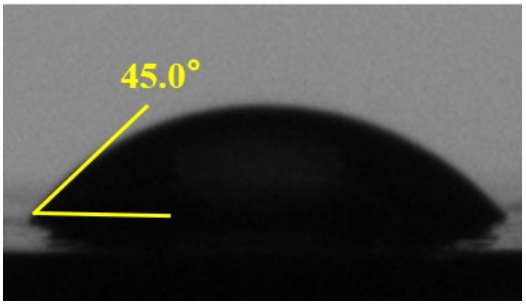

Fig. S22. Water contact angle on UiO-67-CF_3-0.

Table S1 Comparison of photocatalytic CO_2 reduction performance with MOFs and MOFs-based composite photocatalysts in similar reaction conditions.

Photocatalyst	Reaction condition	Light source	Yield of products	Refs.
PCN-222-Cu@TpPa-1 (1:2)	CO_2, H_2O	a xenon lamp light source (300 W, AM 1.5 G filter, 102 mW/cm^2)	CO: 90.57 μmol/(g·h); CH_4: 21.27 μmol/(g·h)	[5]
Cu-MOF–Fcdc-20%	CO_2, H_2O	300 W Xe lamp	CO: 8.61 μmol/(g·h)	[6]
$Cs_3Bi_2Br_9$/MOF525Co	CO_2, H_2O vapor	300 W Xe lamp	CO: 61.2 μmol/(g·h); CH_4: 0.3 μmol/(g·h)	[7]
In-MOF@TP-TA	CO_2, H_2O	300 W Xe lamp	CO: 25 μmol/(g·h); CH_4: 11.67 μmol/(g·h)	[8]
TOC/Cu-MOF	CO_2, H_2O	300 W Xe lamp	CO: 23.01 μmol/(g·h)	[9]
$CsPbBr_3$@Pb-MOF-2	CO_2, H_2O vapor	300 W Xe lamp	CO: 107 μmol/(g·h)	[10]
Co-PMOF/GR	CO_2, H_2O	A 300 W xenon lamp with a 420 nm UV-cut filter	CO: 20.25 μmol/(g·h); CH_4: 1.16 μmol/(g·h)	[11]
$MAPbBr_3$/Pb-MOF	CO_2, H_2O	300 W Xe lamp	CO: 7.3 μmol/(g·h)	[12]
$BiOIO_3$/Zn-MOF-15(BOIOZ-15)	CO_2, H_2O	300 W Xe lamp	CO: 58.82 μmol/(g·h)	[13]
IRMOF-74-IV-PBHB45%-Cu	CO_2, H_2O	300 W Xe lamp	CO: 85.1 μmol/(g·h)	[14]
UiO-66-6	CO_2, H_2O	300 W Xe lamp with a $\lambda > 420$ nm filter	CO: 1.33 μmol/(g·h)	[15]
Co-MOF/Cu_2O	CO_2, H_2O vapor	300 W Xe lamp with a $\lambda > 420$ nm filter	CO: 3.83 μmol/(g·h)	[16]
CTU/CdS-P25	CO_2, H_2O	300 W Xe lamp	CO: 2.38 μmol/(g·h)	[17]
3-RhB@Zr-MOF	CO_2, H_2O vapor	300 W Xe lamp with a $\lambda > 400$ nm filter	CO:2.57 μmol/(g·h)	[18]
$CsPbBr_3$@Au@PCN-333(Al)	CO_2, H_2O	A 150 W Xe lamp (Zolix) equipped with an AM 1.5G filter and 420 nm optical filter	CO: 62.05 μmol/(g·h)	[19]
$Al_2(OH)_2$TCPP-Co MONs	CO_2, H_2O vapor	300 W Xe lamp, 780 nm > $\lambda \geq$ 320 nm	CO: 118.7 μmol/(g·h)	[20]
TpPa@IEF	CO_2, H_2O vapor	an LED light	CO: 78.87 μmol/(g·h)	[21]
IEF-11@Zr-TCPP	CO_2, H_2O vapor	LED lamp	CO: 201.71μmol/(g·h)	[22]
Au@PCN-222	CO_2, H_2O	xenon lamp equipped with a band-cut filter ($\lambda \geq 420$ nm)	CO: 29.1 μmol/(g·h) CH_4: 2.5 μmol/(g·h)	[23]
Co_2L@NH_2-MIL-125	CO_2, H_2O	300 W Xe lamp($\lambda >$ 420 nm)	CO: 27.95 μmol/(g·h)	[24]
UiO-66/Ni-TCPP@P25	CO_2, H_2O	300 W xenon lamp	CO: 14.64 μmol/(g·h)	[25]

NH_2-MIL-125	Simulated air and flue gas environment (CO_2, N_2, and O_2)	300 W xenon lamp	CO: 39.915 μmol/(g·h)	[26]
Pd/Bi-MOF	CO_2, H_2O vapor	300 W xenon lamp	CO: 8.24 μmol/(g·h); CH_4: 0.49 μmol/(g·h)	[27]
Bi-BTC-BiOBr/$CdIn_2S_4$	CO_2, H_2O vapor	300 W xenon lamp	CO: 30.18 μmol/(g·h); CH_4: 1.5 μmol/(g·h)	[28]
Co_2-MOF-NH_2-10@TTA-TTB	CO_2, H_2O vapor	300 W Xe lamp	CO: 70.33 μmol/(g·h)	[29]
NZZ0.14/TTCOF	CO_2, H_2O vapor	PLS-SXE300+ xenon lamp	CO: 7.01 μmol/(g·h); CH4: 2.50 μmol/(g·h)	[30]
MOF-Co/Cu/Fe	CO_2, H_2O	a full-spectrum Xe lamp (300 W, λ 300–2500 nm)	CO: 17.06 μmol/(g·h)	[31]
MOF-808/RGO-5	CO_2, H_2O vapor	Xe lamp (300 W)	CO: 14.35 μmol/(g·h); CH_4: 0.0625 μmol/(g·h)	[32]
BOB/BM-2	CO_2, H_2O	Xe lamp (300 W)	CO: 22.35 μmol/(g·h)	[33]
Ni-BDCMOF/MnO_2	CO_2, H_2O	Xe lamp (300 W)	CO: 9.495 μmol/(g·h) CH_4: 3.92 μmol/(g·h)	[34]
$BiOIO_3$/Bi-MOF	CO_2, H_2O	Xe lamp (300 W)	CO: 21.26 μmol/(g·h)	[35]
BMCN/300	CO_2, H_2O	Xe lamp (300 W)	CO: 51.3 μmol/(g·h); CH_4: 165.3 μmol/(g·h)	[36]
BOC/Bi-MOF	CO_2, H_2O	Xe lamp (300 W)	CO: 363.74 μmol/(g·h)	[37]
$Cs_3Bi_2Br_9$@UiO-66	CO_2, H_2O vapor	Xe lamp (300 W)	CO: 41.73 μmol/(g·h); CH_4: 6.17 μmol/(g·h)	[38]
M68N@In-TCPP	CO_2, H_2O	outdoor natural sunlight	CO: 61.2 μmol/(g·h); HCOOH: 397.5 μmol/(g·h)	[39]
UiO-67-*o*-$(CH_3)_2$	CO_2, H_2O	Xe lamp (300 W)	CO:178 μmol/(g·h)	[40]
CdS/MIL-53 (Fe/Mn)	CO_2, H_2O vapor	Xe lamp (300 W)	CO:2.67 μmol/(g·h)	[41]
MIL-125(Ti) NS\ZnTcPc	CO_2, H_2O vapor	Xe lamp (300 W)	CO: 450.8 μmol/(g·h); CH_4: 55.9 μmol/(g·h)	[42]
NH_2-MIL-125/DE-60 %	CO_2, H_2O vapor	($320 \leq \lambda \leq 780$ nm; light intensity 248 mW cm^{-2}) lamp	CO:7.36 μmol/(g·h)	[43]
[DMC@cMOF]-PVK	CO_2, H_2O	Xe lamp (300 W)	CO:133.36 μmol/(g·h)	[44]

11%$MAPbBr_3$@MIL-101（Cr）	CO_2, H_2O	Xe lamp (300 W)	CO: 16.9 μmol/(g·h); CH_4: 80.3 μmol/(g·h)	[45]
g-C_3N_4/TNTAs	CO_2, H_2O vapor	Xe lamp (300 W)	CO: 29.69 μmol/(cm^2·h); CH_4: 2.88 μmol/(cm^2·h)	[46]
15%PCN-224(Cu)/TiO_2	CO_2, H_2O	Xe lamp (300 W)	CO: 37.21 μmol/(g·h); CH_4: 0.21 μmol/(g·h)	[47]
UiO-67-CF_3-50	CO_2, H_2O	Xe lamp (300 W)	CO: 171.4μmol/(g·h)	This work

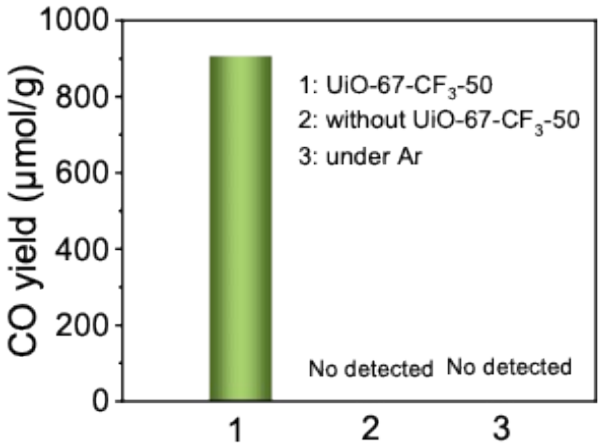

Fig. S23. CO yields under different photocatalytic reaction conditions.

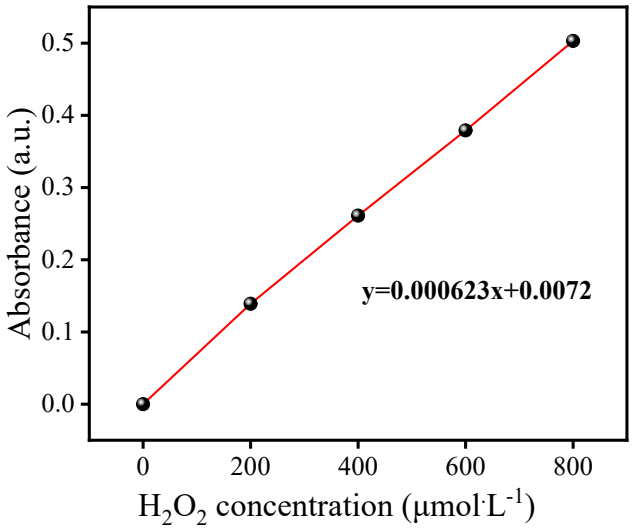

Fig. S24. Calibration curve for the quantification of H_2O_2.

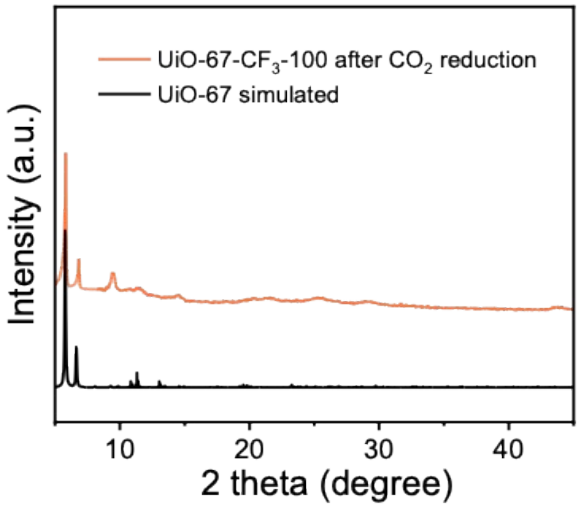

Fig. S25. PXRD pattern of UiO-67-CF_3-100 after photocatalysis.

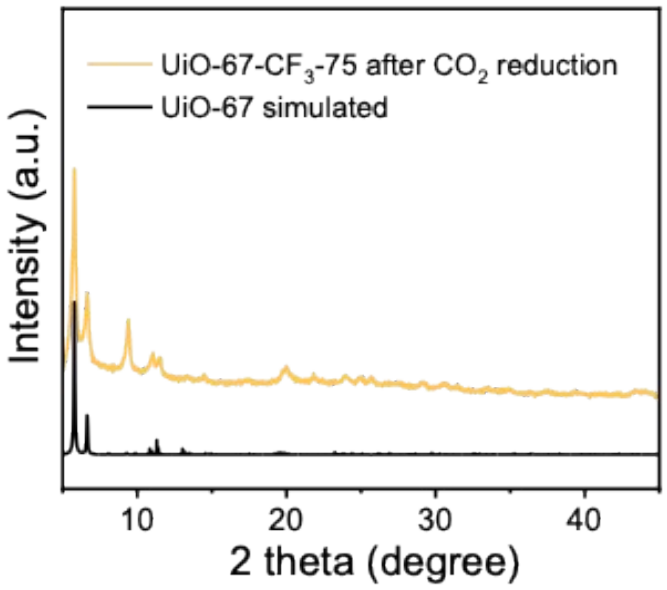

Fig. S26. PXRD pattern of UiO-67-CF_3-75 after photocatalysis.

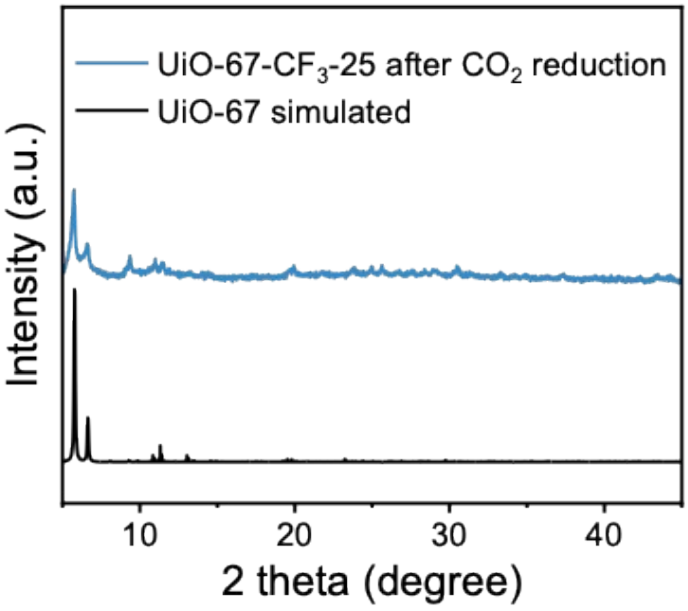

Fig. S27. PXRD pattern of UiO-67-CF_3-25 after photocatalysis.

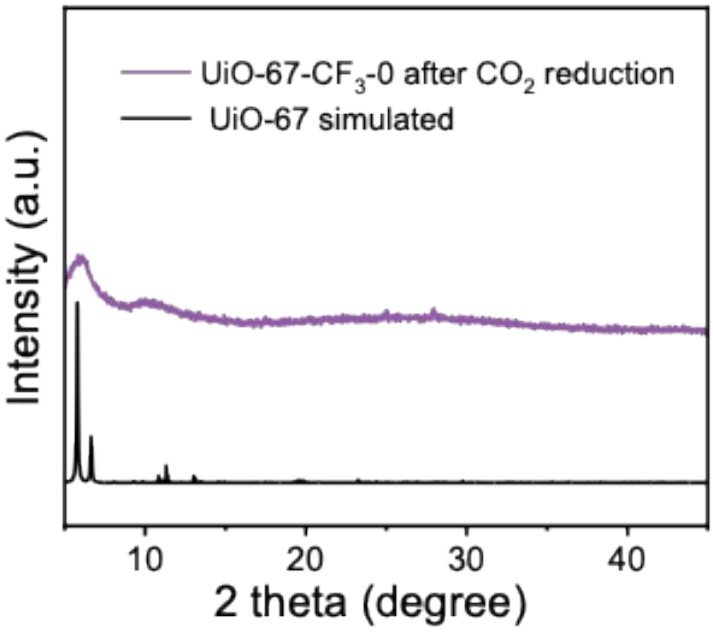

Fig. S28. PXRD pattern of UiO-67-CF_3-0 after photocatalysis.

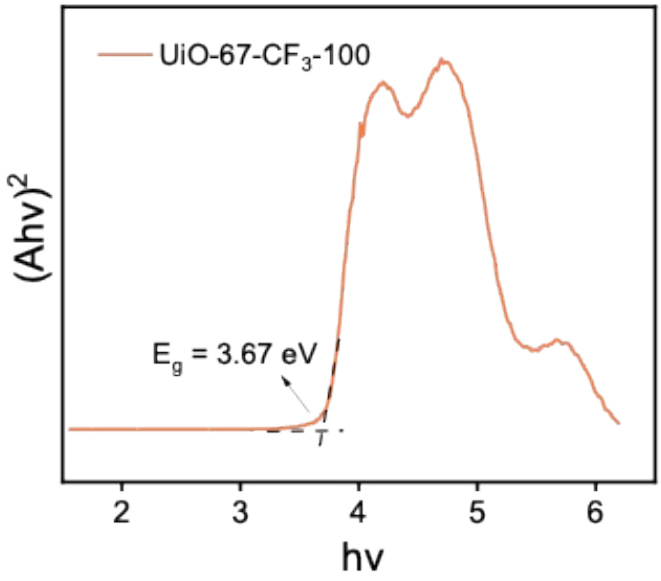

Fig. S29. Kubelka–Munk analysis of UiO-67-CF_3-100.

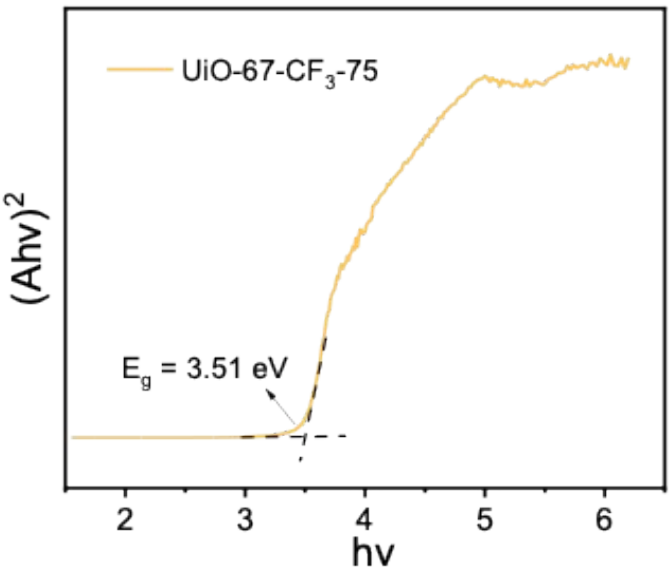

Fig. S30. Kubelka–Munk analysis of UiO-67-CF_3-75.

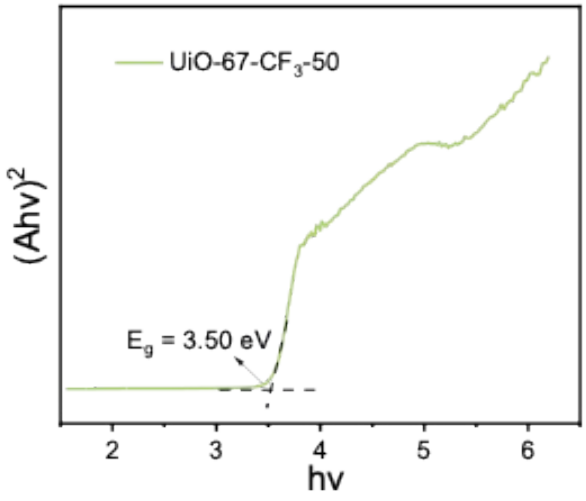

Fig. S31. Kubelka–Munk analysis of UiO-67-CF_3-50.

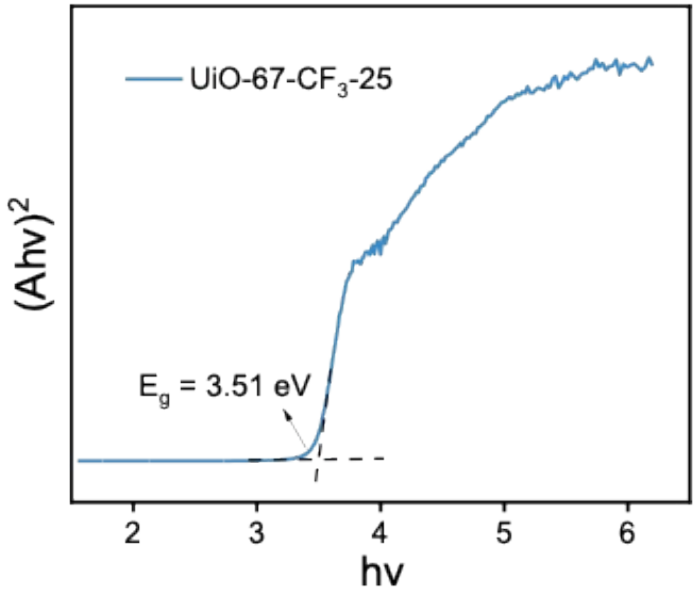

Fig. S32. Kubelka–Munk analysis of UiO-67-CF_3-25.

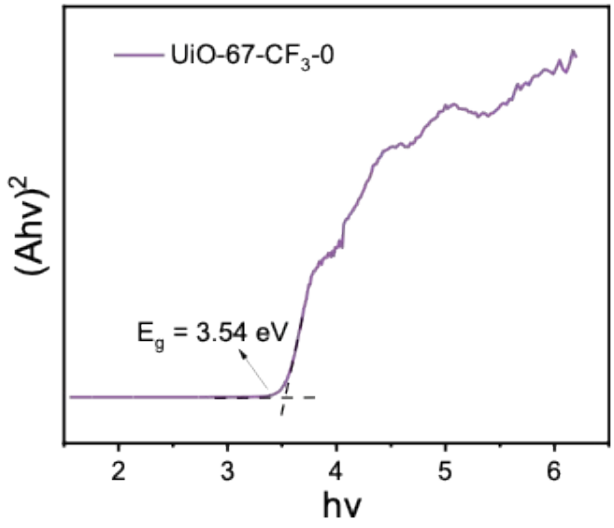

Fig. S33. Kubelka–Munk analysis of UiO-67-CF_3-0.

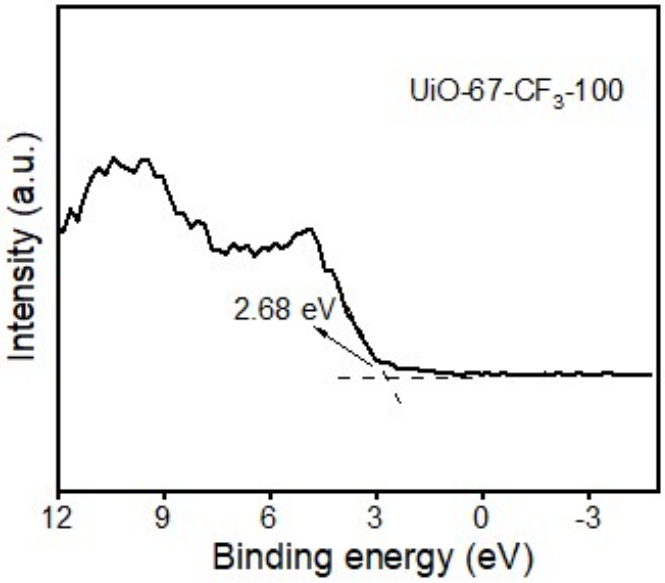

Fig. S34. XPS valence band potential of UiO-67-CF_3-100.

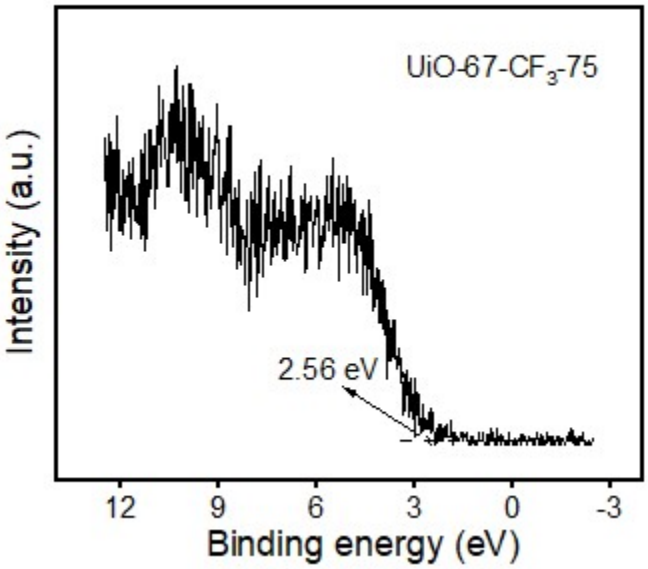

Fig. S35. XPS valence band potential of UiO-67-CF_3-75.

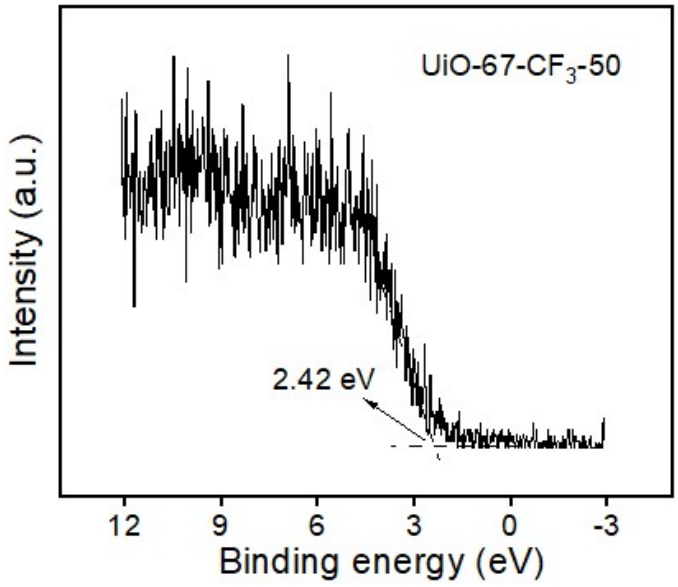

Fig. S36. XPS valence band potential of UiO-67-CF_3-50.

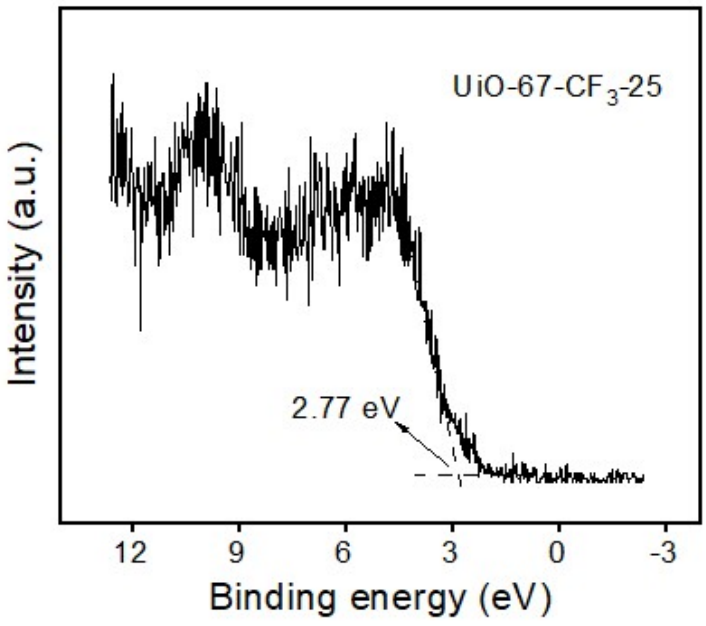

Fig. S37. XPS valence band potential of UiO-67-CF_3-25.

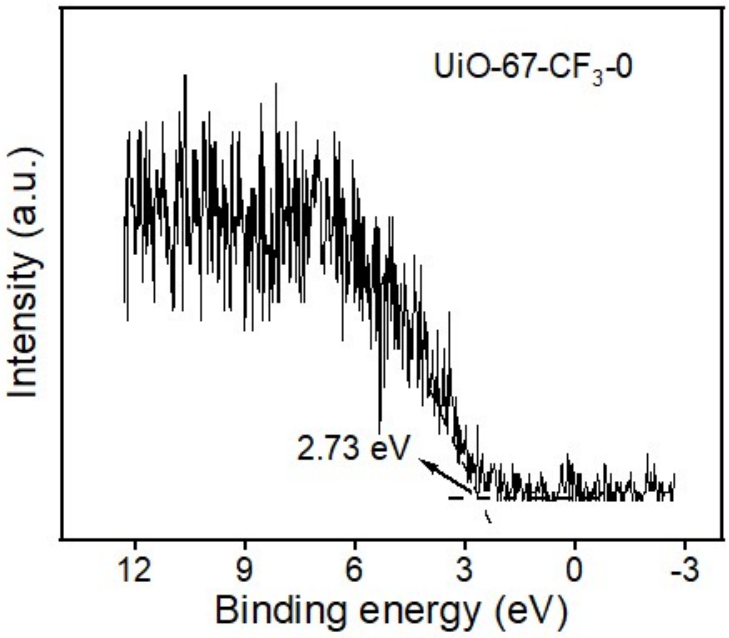

Fig. S38. XPS valence band potential of UiO-67-CF_3-0.

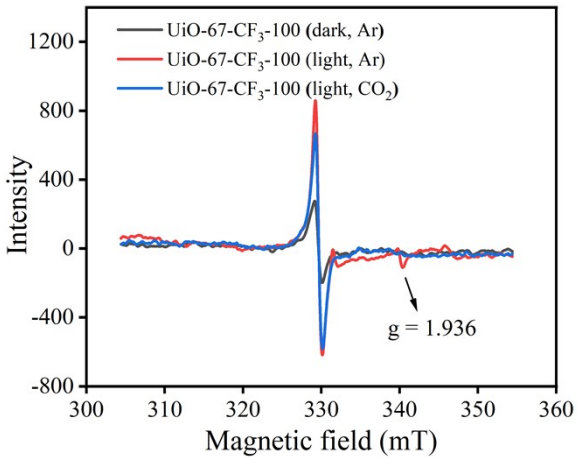

Fig. S39 EPR spectra of UiO-67-CF_3-100 under different condition.

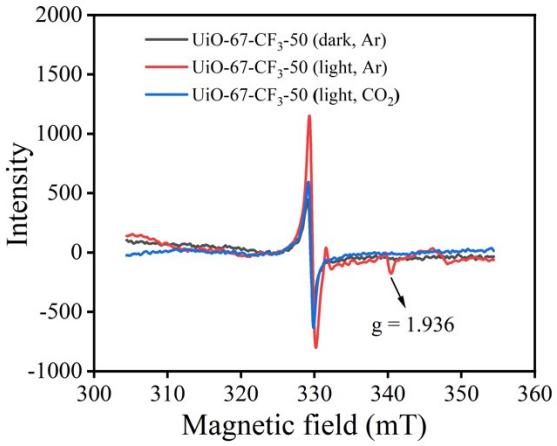

Fig. S40 EPR spectra of UiO-67-CF_3-50 under different condition.

6. References

[1] K. Wang, H. Huang, X. Zhou, Q. Wang, G. Li, H. Shen, Y. She and C. Zhong, *Inorg. Chem.,* 2019, **58**, 5725-5732.

[2] M. J. Frisch, G. W. Trucks, H. B. Schlegel, G. E. Scuseria, M. A. Robb, J. R. Cheeseman, G. Scalmani, V. Barone, G. A. Petersson, H. Nakatsuji, X. Li, M. Caricato, A. V. Marenich, J. Bloino, B. G. Janesko, R. Gomperts, B. Mennucci, H. P. Hratchian, J. V. Ortiz, A. F. Izmaylov, J. L. Sonnenberg, D. Williams-Young, F. Ding, F. Lipparini, F. Egidi, J. Goings, B. Peng, A. Petrone, T. Henderson, D. Ranasinghe, V. G. Zakrzewski, J. Gao, N. Rega, G. Zheng, W. Liang, M. Hada, M. Ehara, K. Toyota, R. Fukuda, J. Hasegawa, M. Ishida, T. Nakajima, Y. Honda, O. Kitao, H. Nakai, T. Vreven, K. Throssell, J. A. Montgomery, Jr., J. E. Peralta, F. Ogliaro, M. J. Bearpark, J. J. Heyd, E. N. Brothers, K. N. Kudin, V. N. Staroverov, T. A. Keith, R. Kobayashi, J. Normand, K. Raghavachari, A. P. Rendell, J. C. Burant, S. S. Iyengar, J. Tomasi, M. Cossi, J. M. Millam, M. Klene, C. Adamo, R. Cammi, J. W. Ochterski, R. L. Martin, K. Morokuma, O. Farkas, J. B. Foresman and D. J. Fox Gaussian 16, Revision C.01; Gaussian, Inc.: Wallingford, CT, 2019.

[3] J.-D. Chai and M. Head-Gordon, *Phys. Chem. Chem. Phys.,* 2008, **10**, 6615.

[4] F. Weigend and R. Ahlrichs, *Phys. Chem. Chem. Phys.,* 2005, **7**, 3297.

[5] Z. Wu, W. Li, L. Hou, Q. Wei, H. Yang, Y. Jiang and D. Tang, *Sep. Purif. Technol.*, 2023, **311**, 123322.

[6] H. Yang, M. Zhang, Z. Guan and J. Yang, *Catal. Sci. Technol.*, 2023, **13**, 6238-6246.

[7] N. Li, X.-P. Zhai, B. Ma, H.-J. Zhang, M.-J. Xiao, Q. Wang and H.-L. Zhang, *J. Mater. Chem. A*, 2023, **11**, 4020–4029.

[8] L. Wang, J. Mao, G. Huang, Y. Zhang, J. Huang, H. She, C. Liu, H. Liu and Q. Wang, *Chem. Eng. J.*, 2022, **446**, 137011.

[9] Q. Wu, H. Ma, Y. Wang, J. Chen, J. Dai, X. Xu and X. Wu, *ACS Appl. Mater. Interfaces*, 2022, **14**, 54328–54337.

[10] Y. Hou, M. Dong, J. He, J. Sun, C. Sun, X. Li, X. Wang and Z. Su, *Inorg. Chem. Front.*, 2023, **10**, 5098–5110.

[11] L. Cheng, C. Wu, H. Feng and H. Liu, *Catal. Sci. Technol.*, 2022, **12**, 7057–7064.

[12] D.-Y. Zhou, W.-T. Su, X.-Y. Li, T. Hong, G.-Y. Pan, M.-L. Xu, F.-T. Liu and K. Li, *J. Mater. Chem. C*, 2023, **11**, 15700–15705.

[13] Y. Niu, J. Jiang, X. Fang, F. Zhang and Y. Wang, *Solid State Sci.*, 2024, **147**, 107407.

[14] T.-C. Li, X.-J. Kong, Y. Xie, T. He, G.-R. Si, X.-Y. Li, W. Wu, M. Zhao and J.-R. Li, *Sep. Purif. Technol.*, 2022, **292**, 121080.

[15] Y. He, C. Li, X.-B. Chen, Z. Shi and S. Feng, *ACS Appl. Mater. Interfaces*, 2022, **14**, 28977–28984.

[16] W.-W. Dong, J. Jia, Y. Wang, J.-R. An, O.-Y. Yang, X.-J. Gao, Y.-L. Liu, J. Zhao and D.-S. Li, *Chem. Eng. J.*, 2022, **438**, 135622.

[17] R. Lian, L. Wang, Y. Gao, J. Zhang, Q. Mei and Q. Wang, *J. Alloys Compd.*, 2022, **924**, 166590.

[18] O.-Y. Yang, X.-J. Gao, G.-D. Qi, Y. Wang, W.-W. Dong, Z.-F. Tian, J. Zhao, D.-S. Li and Q. Zhang, *ACS Appl. Energy Mater.*, 2023, **6**, 334–341.

[19] J.-N. Huang, Y.-J. Dong, H.-B. Zhao, H.-Y. Chen, D.-B. Kuang and C.-Y. Su, *J. Mater. Chem. A*, 2022, **10**, 25212–25219.

[20] R. Peng, Y. Guo, J. Liu, H. Wang, Z. Li, X. Xuan, Y. Zhao and J. Wang, *J. Mol. Liq.*, 2023, **383**, 122153.

[21] R.-G. Yang, Y.-M. Fu, X. Meng, L. Xue, Z. Zhou, Y.-O. He, J.-X. Qu, H.-N. Wang and Z.-M. Su, *Inorg. Chem. Front.*, 2023, 10, 3699–3705.

[22] J.-R. Liu, Y.-M. Fu, Y.-O. He, W.-T. Ju, X. Meng, H.-N. Wang and Z.-M. Su, *J. Solid State Chem.*, 2025, **347**, 125323.

[23] T. Huang, J. Han, Z. Li, Y. Hong, X. Gu, Y. Wu, Y. Zhang and S. Liu, *Angew. Chem. Int. Ed.*, 2025, **64**, e202500269.

[24] H.-F. Wang, H. Yuan, S.-Z. Feng, B.-X. Dong and D.-C. Zhong, *Inorg. Chem.*, 2024, **63**, 22033–22039.

[25] R. Wang, W. Cheng, H. Wang, Q. Mei, X. Li, B. Bai and Q. Wang, *J. Environ. Chem. Eng.*, 2025, **13**, 115360.

[26] M. Que, P. Ma, Y. Wang, Y. Sun, X. Bai, L. Gao, J. Chen, J. Wei and H. Li, *J. Colloid Interface Sci.*, 2025, **683**, 116–124.

[27] C. Ma, Z. Zhong and Q. Xiang, *Mol. Catal.,* 2025, **571**, 114700.

[28] M. Shen, Y. Li, T. Luo, Z. Wang, M. Zhou, Y. Wang, S. Xu and Z. Li, *Sep. Purif. Technol.*, 2025, **355**, 129713.

[29] Y.-C. Wang, W.-J. Shi, J.-H. Zhang, W.-X. Tao, D.-C. Zhong and T.-B. Lu, *Chem. Eng. J.*, 2025, **517**, 164327.

[30] Y. Qiu, C. Jiang, X. Xin, Y.-Y. Li, H. Wang, J. Xu, H. Lin, L. Wang and V. Turkevich, *ACS Appl. Nano Mater.*, 2024, **7**, 11234–11247.

[31] H. Han, H. Cui, J. Wang, K. Ge and Y. Yang, *ChemistrySelect*, 2024, **9**, e202403927.

[32] M. Song, J. Li, M. Xu, Z. Xu, X. Song, X. Liu, J. Zhang, Y. Yang, X. Xie, W. Zhou and P. Huo, *J. Colloid Interface Sci.*, 2024, **668**, 471–483.

[33] S. Wu, M. Xu, L. Ai, Q. Ma, C. Leng, N. Guo, H. Fan and L. Wang, *J. Colloid Interface Sci.*, 2026, **702**, 138807.

[34] H. Haroon, W. Ji, Q. Xiang, M. Wahid and J. Li, *ChemistrySelect*, 2025, **10**, e202405803.

[35] Y. Niu, J. Jiang, X. Zhou, Y. Wang, J. Ma and F. Zhang, *Solid State Sci.*, 2024, **156**, 107670.

[36] Y. Zou, E. Rukundo, S. Feng, X. Chen and Y. Liu, *Chem. Eng. J.*, 2024, **492**, 152435.

[37] H. Shi, M. Xu, C. Leng, L. Ai, L. Wang, H. Fan and S. Wu, *J. Colloid Interface Sci.*, 2025, **680**, 1067–1078.

[38] Z. Fang, X. Yue and Q. Xiang, *Small*, 2024, **20**, 2401914.

[39] Z. Cai, H. Liu, J. Dai, B. Li, L. Yang, J. Wang and H. Zhu, *Nat. Commun.*, 2025, **16**, 2601.

[40] K. Wang, B. Yan, B. Zhou, Y. Zhang, G.-L. Lin, T.-S. Zhang, M. Zhou, H.-M. Shen, Y.-F. Yang, J. Xia,

H. Li and Y. She, *ACS Appl. Mater. Interfaces*, 2024, **16**, 33601–33610.

[41] R. Xuan, J. Chen, Y. Dou, Z. Jiang, X. Li, D. Ding, C. Wang, J. Yan and L. Sun, *J. Environ. Chem. Eng.*, 2025, **13**, 115293.

[42] Y. Jiao, Y. Chen, L. Liu, X. Yu and G. Tian, *Small*, 2024, **20**, 2309094.

[43] Y. Wen, C. Qian, B. Cui, B. Tian, C. Li, H. Li, F. Yuan and Z. Sun, *J. Colloid Interface Sci.*, 2025, **697**, 137970.

[44] K. Yuan, K. Tao, T. Song, Y. Zhang, T. Zhang, F. Wang, S. Duan, Z. Chen, L. Li, X. Zhang, D. Zhong, Z. Tang, T.-B. Lu and W. Hu, *J. Am. Chem. Soc.*, 2024, **146**, 6893–6904.

[45] J. Zhang, W. Zhou, J. Chen and Y. Li, *Catalysts*, 2024, **14**, 590.

[46] M. A. Hossen, R. R. Ikreedeegh, A. A. Aziz and M. Tahir, *Next Mater.*, 2025, **9**, 100951.

[47] L. Wang, P. Jin, J. Huang, H. She and Q. Wang, *ACS Sustainable Chem. Eng.*, 2019, **7**, 15660–15670.